A Mode Shape Sensitivity-based Method for Damage Detection of Structures with Closely-spaced Eigenvalues

Abstract

A new optimisation problem is proposed to facilitate a fast and reliable damage detection of structures with closely-spaced eigenvalues. The first stage of the proposed method identifies the most probable defective elements resulting in the elimination of healthy members from further investigation. This will further reduce the computational efforts of computing damage indices regarding the defective elements. The second stage of the proposed method exploits the proposed objective function to update the damage indices of the identified defective elements from the first stage. Two truss structures with multiple damaged elements in different damage scenarios are studied where measurements with different levels of noise are used as input to the proposed algorithm. Numerical results and comparison with previous studies demonstrate the superiority of the proposed method in damage detection of structures with closely-spaced eigenvalues.

Keywords: Structural health monitoring, Damage detection, Modal residual vector, Closely-spaced eigenvalues, Optimisation algorithm

https://doi.org/10.1016/j.measurement.2021.110644

1. Introduction

Structural health monitoring (SHM) ensures the safety and reliability of large-scaled structures such as bridges, high rise buildings, and cultural heritage structures. Therefore, a great deal of attention has given to developing new damage detection strategies over the past decades.

There are generally two types of structural damage detection techniques which are: the local and global methods. Some of the well-known local methods include ultrasonic testing (UT), thermographic testing, infrared thermography testing, radiographic testing, acoustic emission testing (AE), shearography testing, visual testing (VT) or visual inspection (VI), optical testing, liquid penetrant testing, magnetic particle testing and electromagnetic testing [1, 2, 3, 4, 5]. These techniques, that are usually used for detection and characterisation of damage in a confined area on the structure, can be either destructive or Non-destructive. Non-destructive Damage Testing (NDT) approaches are usually referred to non-intrusive techniques [6]. In contrast, intrusive techniques may cause destruction of some parts of the materials to asses their quality. For example, using resistograph to pierce into the wood sections for wood quality assessment [7]. While local methods are limited in terms of conducting damage detection on a confined area of structures, global methods, usually, termed as vibration-based techniques, are used for damage detection in a large area on structures through studying structural vibration data [8, 9, 10, 11]. Since the vibration-based methods do not require measurements at or near the damage site, they do not need any inspection of local areas on the structure. It is known that damage can modify the structural modal information such as mass, stiffness and damping matrices which can further change the structural modal properties such as natural frequency, mode shapes, their derivatives, etc [12, 13]. Therefore, damage can be detected through comparing the modal information of the intact and damaged structures. For example, structural natural frequencies [14], damping [15], mode shapes and mode shapes curvatures [16], the modal strain energy [17], the dynamic flexibility and dynamic flexibility curvatures [18, 19, 20, 21, 22], the anti-resonances [23], the Frequency Response Function (FRF) and its curvatures [22, 24, 25, 26, 27, 28], have been used widely to this end.

It is known that damage detection of spatial structures is challenging due to the presence of the closely-spaced eigenvalues problem. As such, most of the global techniques are only capable of damage localisation when applied to these types of structures. In recent decades, many researchers have applied vibration-based damage detection methods to spatial structures due to their high accuracy [29, 30, 31].

Optimisation-based damage detection strategies benefit largely from the advances in the mathematics and computer technologies in recent years. Kang et al. [32] combined particle swarm optimisation (PSO) algorithm with the artificial immune system algorithm to develop an immunity enhanced particle swarm optimisation (IEPSO) algorithm to be used for damage detection in truss structures where the objective function was constructed using structural natural frequencies and mode shapes. Khatir and Wahab [33] proposed a method by mixing the eXtended Finite Element (XFEM) and the eXtended IsoGeometric Analysis (XIGA) with Particle Swarm Optimisation (PSO) and Jaya algorithm to identify the crack site in structures. Beetle swarm optimisation (BSO) is a meta-heuristic algorithm proposed by Jiang et al. [34] to detect both damage localisation and quantification through optimising an objective function based on measured modal data. Sometimes, the optimisation problem regarding updating damage indices can converge to a local solution which is not of course a desired solution. The disturbed PSO (DPSO) uses the disturbance to make particles escape from local minima in PSO algorithm which was proposed by Wei et al. [35], and used for structural damage identification. Another challenge relates to proposing novel objective functions for damage detection purposes. For instance, Dinh-Cong et al. [36] constructed a new objective function based on the flexibility variations vector of the structure and further used a modified differential evolution (MDE) algorithm to update the fitness function.

Some researchers exploit optimisation-based algorithms for solving damage detection problems in two stages. Accordingly, the first stage is dedicated to damage localisation that aims to reduce the dimensionality of the search space regarding the second stage, i.e. damage quantification. The second stage of such method, applies optimisation algorithms to work out the extent of damage in identified defective elements from the first stage. Therefore, these methods are usually referred to as “hybrid” methods. Naderi et al. [37] have proposed a two-stage damage detection method applied to determinate truss structures using the first natural frequency and its corresponding mode shape vector. Accordingly, in the first stage, the Modal Residual Force Vector (MRFV) regarding the first mode is applied to the structure as an external nodal force vector. Damaged members are then detected based on the magnitude of the induced local nodal force vector for each member. As such, a member is regarded as defective if the magnitude of this force vector is obtained non-zero. In the second stage, the damage severity of damaged members, detected in the first stage, is worked out through establishing a new relationship between the force and displacement. In another two-stage method proposed by Vo-Duy et al. [38], the modal strain energy index is used in the first stage for identifying defective elements. Then, an improved differential evolution algorithm is utilised to detect the extent of damage in laminated composite structures. Xiang and Liang [39] have developed a two-stage method for damage detection in plate structures based on the 2-D wavelet transform and the PSO algorithm. The proposed method of this paper is also a two-stage method the first stage of which is dedicated to identifying the most probable defective elements.

Sometimes two modal frequencies of the structure are so close to each other that they can be regarded as one mode. This phenomenon is termed as the closely-spaced eigenvalues situation. This can happen in multiple modes of some complex structures such as spatial trusses. Existence of such a problem can bring about uncertainty and variability in the structural response making the process of damage detection in these structures difficult. It is known that even small perturbations in geometry, mass, or stiffness distributions of some structures can result in either initiation of closely-spaced eigenvalue problem or worsening the situation by increasing the number of the modes suffering from this phenomenon [40, 41]. This phenomenon, however, neither is well understood nor specifically much mentioned in the literature of structural dynamics. Such observation though appears indirectly in some theoretical papers where the original treatment of such problem is intended [42, 43]. It is well understood, however, from the theory of structural modification (SM) and the system equivalent reduction expansion process (SEREP) that an experimentally obtained mode shape can be smoothed using a linear combination of mode shapes obtained from a finite element (FE) model of the structure. This principle is termed as the principle of local correspondence (LC) [44]. Brincker and Lopez-Aenlle [42] showed, based on the LC principal, that in the case of a set of two closely-spaced eigenvalues, the mode shapes become highly sensitive to small changes of the system. In such a case, a linear transformation can be established between the set of perturbed mode shapes cluster Ψ and unperturbed mode shapes cluster Φ, provided that the two closely-spaced eigenvalues have a reasonable frequency distance to all other eigenvalues of the system. Such a mapping is in the form of a rotation in the initial subspace defined by the two mode shapes that can describe the significant changes of the system (Fig. 2). This property is used in this paper to construct an objective function in the second stage where an optimisation problem is solved for damage quantification.

2. A criteria for repeated closely spaced eigenvalues(FDI)

Although closely-spaced eigenvalues are not as common as well-separated eigenvalues, they do typically occur in complex structures such as spatial truss structures [43]. In this study, we show that the closely-spaced eigenvalues phenomenon can make some damage detection methods ineffective for such structures. A metric in here is introduced to characterise the extent of the close-modes phenomenon in an undamped structure based on the concept introduced for damped structures in [43]. The proposed concept is described as follows:

Two eigenvalues $\omega_i = \omega$ and $\omega_j = \omega + \Delta\omega$ are considered closely-spaced if $\Delta\omega = \omega_j - \omega_i$ is small compared with ω [42]. The frequency disparity index (FDI) is then calculated, for the pair (f_i, f_j) equivalent to $(\omega_i/2\pi, \omega_j/2\pi)$ regarding an undamped structure as follows:

$$\mathrm{FDI}_{i,j}\% = \left| \frac{f_j - f_i}{f_i} \right| \times 100 \tag{1}$$

Accordingly, two modes are characterised as

1. Well-separated: if and only if $\mathrm{FDI}_{i,j} > 10\%$,

https://doi.org/10.1016/j.measurement.2021.110644

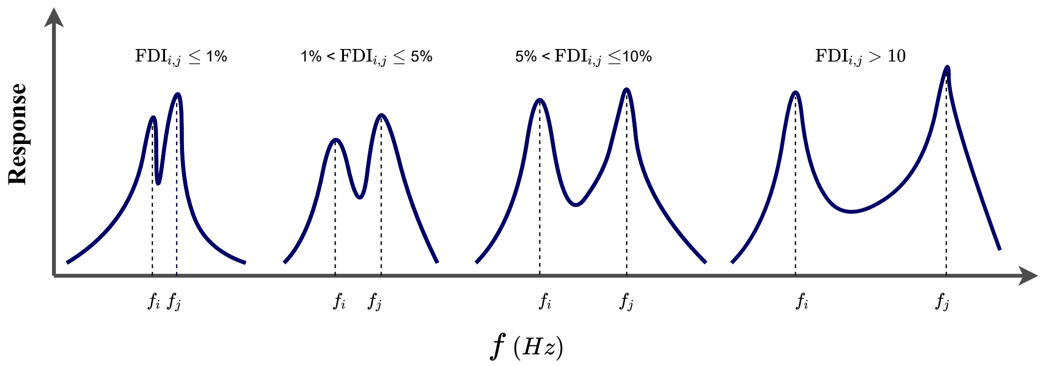

Figure 1: Schematic presentation of two closely-spaced eigenvalues.

2. Separated: if and only if $5\% < \mathrm{FDI}_{i,j} \leq 10\%$,
3. Close: if and only if $1\% < \mathrm{FDI}_{i,j} \leq 5\%$, and
4. Very close: if and only if $\mathrm{FDI}_{i,j} \leq 1\%$.

Fig. 1 shows different states of two closely-spaced eigenvalues schematically.

In case $\omega_i = \omega$ and $\omega_j = \omega + \Delta\omega$, Equation 1 reduces to

$$\mathrm{FDI}_{i,j}\% = \left|\frac{\Delta\omega}{\omega}\right| \times 100. \tag{2}$$

When $(\Delta\omega/\omega) \to 0$, we can say that we have two repeated eigenvalues. We set an approximate equivalent for this when $\mathrm{FDI}_{i,j} \leq 0.01\%$.

3. The proposed damage detection method

3.1. Damage localisation using modal residual vector based indicator (MRVBI)

A method is presented in this section for identifying defective elements in the first stage [12, 45, 46]. Let M and K be respectively the mass and stiffness matrices of a healthy n-DOF structure. The following generalised eigenvalue problem holds:

$$\left(K - \omega_j^2 M\right)\varphi_j = 0 \tag{3}$$

where ω_j and φ_j are the j^{th} natural frequency and its corresponding mode shape vector, respectively. Rewriting (3) for damaged structure we have:

$$\left(K_{\mathrm{d}} - \omega_{\mathrm{d}j}^2 M_{\mathrm{d}}\right)\varphi_{\mathrm{d}j} = 0 \tag{4}$$

where subscript “d” refers to the damaged structure.

It is assumed that damage can only affect elemental mass and stiffness matrices. As such, the effect of damage on the elemental damping matrix is neglected. Therefore, damage in an element can reduce its stiffness and mass matrices by ΔK^{e} and ΔM^{e}, respectively. Therefore, the total loss of the stiffness and mass of the structure is obtained as follows:

$$\Delta K = \sum_{i=1}^{ne} \Delta K^{\mathrm{e}}{}_{i} \tag{5}$$

and

$$\Delta M = \sum_{i=1}^{ne} \Delta M^{\mathrm{e}}{}_{i} \tag{6}$$

where ne is the number of elements. Therefore, one can obtain the general stiffness K_{d} and mass M_{d} matrices of the damaged structure as follows,

$$K_{\mathrm{d}} = \sum_{i=1}^{ne} K_i^{\mathrm{e}} - \sum_{i=1}^{ne} \Delta K^{\mathrm{e}}{}_{i} \tag{7}$$

and

$$M_{\mathrm{d}} = \sum_{i=1}^{ne} M_i^{\mathrm{e}} - \sum_{i=1}^{ne} \Delta M^{\mathrm{e}}{}_{i} \tag{8}$$

where ne is the number of elements. Substituting (7) and (8) into (4), we obtain:

$$\left(K - \omega_{\mathrm{d}j}^2 M\right) \varphi_{\mathrm{d}j} = \sum_{i=1}^{ne} \Delta K^{\mathrm{e}}{}_{i} \varphi_{\mathrm{d}j} - \sum_{i=1}^{ne} \Delta M^{\mathrm{e}}{}_{i} \omega_{\mathrm{d}j}^2 \varphi_{\mathrm{d}j}. \tag{9}$$

The j^{th} modal residual vector of the structure is thus defined as follows:

$$R_j = \left(K - \omega_{\mathrm{d}j}^2 M\right) \varphi_{\mathrm{d}j} = \Delta K \varphi_{\mathrm{d}j} - \Delta M \omega_{\mathrm{d}j}^2 \varphi_{\mathrm{d}j} \tag{10}$$

where the non-zero components of R_j correspond to the nodal DOFs of the damaged elements . As such, damaged elements are identified based on the connectivity relation between the DOFs and elements. Accordingly, an element is regarded as defective when the entries of R_j corresponding to all of its DOFs are obtained nonzero. Obviously, a more accurate result can be achieved when more and higher mode shapes are used in (10). Note that, in this case, $\sum_j R_j$ is used for damage localisation [45]. Since measuring the higher modes is usually impractical and inaccurate, in this study, the lowest repeated natural frequency (ω_l^*) and its corresponding mode shape (φ_l^*) are only used in (10) for damage localisation. This is mainly due to the fact that the very modal data are further used for damage quantification in the next stage. The mode shape vector of the damaged structure is usually normalised as follows [47, 48]:

$$\bar{\varphi}_{\mathrm{d}l}^* = \frac{\varphi_{\mathrm{d}l}^*}{\varphi_{\mathrm{d}l,max}^*} \tag{11}$$

where $\varphi_{\mathrm{d}l,max}^*$ denotes the maximum component of the repeated mode shape vector $\varphi_{\mathrm{d}l}^*$. Note that the superscript * denotes that the mode shape is repeated and the subscript l indicates that it is the lowest repeated mode of the structure, the subscript "d" also indicates that the mode shape corresponds to a damaged state of the structure. Therefore, we obtain:

$$R_l^* = \left(K - {\omega_{\mathrm{d}l}^*}^2 M\right) \bar{\varphi}_{\mathrm{d}l}^* = \Delta K \bar{\varphi}_{\mathrm{d}l}^* - \Delta M \omega_{\mathrm{d}l}^* \bar{\varphi}_{\mathrm{d}l}^* \tag{12}$$

where R_l^* is modal force error regarding the lowest repeated mode of the structure. Accordingly, the defective elements can be identified via monitoring of the corresponding non-zero components of the obtained vector R_l^* from (12), i.e. the DOFs corresponding to the defective elements.

Note that the stochastic subspace identification method can be used to obtain modal data of a structure experimentally [49]. In this study, the modal data of the structures were obtained through solving the structural modal equation.

3.2. Damage quantification

3.2.1. Setting a new objective function (RMCE)

In this section, a new objective function based on the rotation mapping between closely-spaced eigenvectors (RMCE) of the damaged and healthy structure is constructed. As such, the detail of obtaining such an objective function is explained here.

It is known that the sensitivity of the mode shape φ_i to changes of a parameter u, i.e. $\frac{\partial \varphi_i}{\partial u}$, of a dynamic system can be approximated as [42]:

$$\Delta\varphi_i \cong \Phi \left(\Gamma_{M,i}\Phi^{\mathrm{T}}\Delta M + \Gamma_{K,i}\Phi^{\mathrm{T}}\Delta K\right)\varphi_i \tag{13}$$

in which $\Gamma_{M,i}$ and $\Gamma_{K,i}$ are respectively,

$$\Gamma_{M,i} = [\gamma_r] = \begin{cases} \frac{-\omega_i^2}{m_r(\omega_i^2-\omega_r^2)} \quad \text{if} \quad r \neq i \\ \\ -\frac{1}{2m_i} \quad \text{if} \quad i = r, \end{cases} \tag{14}$$

and

$$\Gamma_{K,i} = [\gamma_r] = \begin{cases} \frac{1}{m_r(\omega_i^2-\omega_r^2)} \quad \text{if} \quad r \neq i \\ \\ 0 \quad \text{if} \quad i = r, \end{cases} \tag{15}$$

where m_i is the i^{th} modal mass. The aforementioned linear transformation can be written as:

$$\Psi = \Phi\left(\tilde{I} + \tilde{T}\right) \tag{16}$$

where $\tilde{I}$ is a truncated identity matrix to compensate for the case when the unperturbed mode shape cluster Φ needs to be bigger than the perturbed mode shape cluster Ψ. Comparing (13) with (16), each of the column vectors ($\tilde{t}_i$) of $\tilde{T}$ is obtained as follows:

$$\tilde{t}_i = \left(\Gamma_{M,i}\Phi^{\mathrm{T}}\Delta M + \Gamma_{K,i}\Phi^{T}\Delta K\right)\varphi_i \tag{17}$$

Taking $T{=}I'{+}T'$ finally proves the existence of the approximate transformation between two corresponding mode shapes clusters as follows:

$$\Psi = \Phi T \tag{18}$$

Note that the transformation is exact in the case of having all modes of the system included in (18). Based on the findings of Brincker and Lopez-Aenlle [42], the transformation T can be obtained as the eigenvectors of the following matrix :

$$\Phi^{\mathrm{T}}\left(-\Delta M + \Delta K/\omega^2\right)\Phi \tag{19}$$

Next, we show that the above discussions hold for only one mode as well. However, there is a catch as the mode shape must be a repeated mode shape. As such, we conclude that (18) and (19) can be used for damage detection when only a repeated mode shape of the structure is identified and used in the equations. Further details will be discussed as follows:

Consider two closely-spaced modes with the frequencies $\omega_1 = \omega$ and $\omega_2 = \omega + \Delta\omega$ (see Section 2). Taking $\Delta\omega$ small compared to the distance of ω to all other modes, i.e. when $\Delta\omega/\omega \to 0$ in (2), following approximations can be made:

1. It can be assumed that the modal masses of the two closely-spaced modes are the same (m).
2. The terms $\omega_2^2/\left(\omega_2^2 - \omega_1^2\right)$ and $1/\left(\omega_2^2 - \omega_1^2\right)$ in (14) and (15) can be approximated respectively as $\omega/(2\Delta\omega)$ and $1/(2\Delta\omega)$.

The weighting terms of (14) and (15) can be then rewritten as follows:

$$\Gamma_{M,1} = \frac{1}{2m}\begin{bmatrix} -1 & 0 \\ 0 & \omega/\Delta\omega \end{bmatrix} \tag{20a}$$

$$\Gamma_{M,2} = \frac{1}{2m}\begin{bmatrix} -\omega/\Delta\omega & 0 \\ 0 & -1 \end{bmatrix} \tag{20b}$$

$$\Gamma_{K,1} = \frac{1}{2m\omega^2}\begin{bmatrix} 0 & 0 \\ 0 & -\omega/\Delta\omega \end{bmatrix} \tag{20c}$$

$$\Gamma_{K,2} = \frac{1}{2m\omega^2}\begin{bmatrix} \omega/\Delta\omega & 0 \\ 0 & 0 \end{bmatrix}. \tag{20d}$$

Therefore, there can be a map established between the subspace constructed by a pair of perturbed and unperturbed eigenvectors as follows:

$$\begin{bmatrix} \psi_1^{\mathrm{T}} \\ \psi_2^{\mathrm{T}} \end{bmatrix} = R \begin{bmatrix} \varphi_1^{\mathrm{T}} \\ \varphi_2^{\mathrm{T}} \end{bmatrix} \tag{21}$$

where

$$R = \begin{bmatrix} cos(\Theta) & sin(\Theta) \\ -sin(\Theta) & cos(\Theta) \end{bmatrix}. \tag{22}$$

Note that R is a rotation matrix with counterclockwise rotation angle Θ (Fig. 2). Since Θ is small, one can approximate $cos(\Theta) \cong 1$ and $sin(\Theta) \cong \Theta$. Therefore,

$$R = \begin{bmatrix} 1 & \Theta \\ -\Theta & 1 \end{bmatrix} \tag{23}$$

where Θ can be approximated as follows:

$$\Theta \cong \frac{\omega}{2m\Delta\omega}\left(\varphi_1^{\mathrm{T}}\Delta M\varphi_2 - \frac{1}{\omega^2}\varphi_1^{\mathrm{T}}\Delta K\varphi_2\right). \tag{24}$$

Therefore, following conclusions can be made:

1. The changes imposed by a perturbation to the system is a rotation of the subspace constructed by the unperturbed mode shapes.
2. The rotation angle is proportional to ΔM and ΔK.
3. The rotation angle is also proportional to the frequency ratio $\omega/\Delta\omega$.

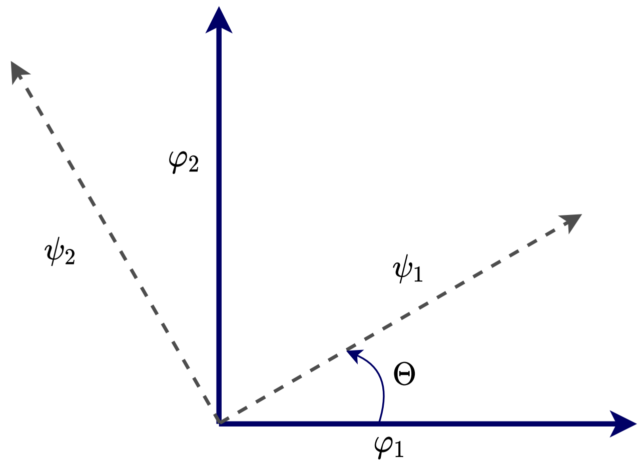

Figure 2: There can be a map established between the subspace constructed by perturbed and unperturbed eigenvectors.

4. Therefore, the smaller $\Delta\omega$, the larger the sensitivity of the mode shapes to ΔM and ΔK.

In this work, damage is simulated as a degradation in either elemental mass or stiffness respectively as follows:

$$M^{\mathrm{e}}_{d,r} = (1 - \alpha_r)\, M^{\mathrm{e}}_r \tag{25}$$

and

$$K^{\mathrm{e}}_{d,r} = (1 - \beta_r)\, K^{\mathrm{e}}_r. \tag{26}$$

where, reiterated, K^{e}_r and M^{e}_r are the stiffness and mass matrices of the r^{th} element in the global coordinate. α_r and $\beta_r \in$ [0 1] represent the elemental mass and stiffness damage parameters with 1 and 0 indicating respectively a complete loss and zero loss of the elemental mass and stiffness. An objective function can be thus constructed for updating damage indices through minimisation. The proposed objective function based on the rotation mapping between closely-spaced eigenvectors of the healthy and damaged structures (RMCE) is, therefore, obtained as follows:

$$\text{RMCE:} \underset{\{\alpha_r\},\, \{\beta_r\}}{min} ||\Psi - \Phi T|| \tag{27}$$

where T is the eignevectors matrix of (19). However, considering the fact that measuring all the mode shapes of the structure is not practically possible, only the first repeated mode of the structure is considered in (19).

3.2.2. Considering the effect of noise

It is inevitable to have noise contamination in measured data. This may further result in obtaining unreliable damage indices. Therefore, it is crucial to study the effect of the measurement noise on the performance of damage detection methods. To this end, the simulated structural modal responses are contaminated by different noise percentage using the following formula [50]:

$$\hat{\delta} = \delta + \frac{\kappa}{100} n_{noise}\, \sigma(\delta) \tag{28}$$

where δ and $\hat{\delta}$ denote respectively the vector of noise-free and noisy measured modal data with standard deviation $\sigma(\delta)$, where k is the noise percentage (0.5% for natural frequency, 10% and 15% for mode shape in the present study). Finally, *noise* is a vector of independent random variables following standard normal distribution.

Note that the noise percentage can be converted to the Signal to Noise Ration (SNR) through the following equation:

$$\text{SNR} = 20\, log\left(\frac{100}{\kappa}\right) \tag{29}$$

Therefore, $\kappa = 10$ and $\kappa = 15$ correspond respectively to SNR$= 20$ and SNR$= 16.48$.

An enhanced particle swarm optimisation algorithm (PSO), embedded in MATLAB Global Optimisation Toolbox, is employed to solve the optimisation problem of this work [51].

3.3. Damage identification accuracy indicators

Different comparative indicators are used in this paper to classify the errors regarding the identified damage indices [52]. To this end, the damage missing error (DME) and false alarm error (FAE) are employed to evaluate the performance of the first phase of the proposed method. The DME is defined as

$$DME = \frac{1}{NT}\sum_{t=1}^{NT} \varepsilon_t^{I}, \text{ for } 0 \leq \text{DME} \leq 1 \tag{30}$$

where NT is the number of real damaged elements in the model. ε_t is the error associated with prediction of the t^{th} defective element–a number equal to zero if the element is truly identified as damaged and 1 if the element is wrongly identified as damaged. Therefore, the damage localisation step is completely accurate when DME $= 0$.

The FAE is defined as follows:

$$FAE = \frac{1}{NF}\sum_{t=1}^{NF} \varepsilon_t^{II}, \text{ for } 0 \leq \text{FAE} \leq 1 \tag{31}$$

where NF is the number of predicted damaged elements in the first stage of the proposed method. ε_t^{II}

takes a value of 0 or 1 indicating respectively that the predicted damaged element is correct or otherwise. Therefore, the damaged elements are perfectly identified when FAE = 0.

In order to asses the results of the second stage of the proposed method, two indicators are introduced as follows:

1. The mean sizing error (MSE): is defined as the mean value of the absolute variations between the measured (or analytical structural parameters) p^a and the predicted structural parameters p^p. MSE over the number of N located damaged elements is defined as follows:

$$\mathrm{MSE} = \frac{1}{N}\sum_{e=1}^{N}|p_e^a - p_e^p|, \text{ for } 0 \leq \mathrm{MSE} \leq \infty \tag{32}$$

2. Relative error (RE): which is the relative form of (32) and is calculated as,

$$\mathrm{RE} = \frac{\sum_{e=1}^{N}|p_e^a| - \sum_{e=1}^{N}|p_e^p|}{\sum_{e=1}^{N}|p_e^a|}, \text{ for } -1 \leq \mathrm{RE} \leq 1. \tag{33}$$

Therefore, more accurate predictions results in smaller values of MSE and RE.

The stages of the proposed method for damage identification are summarised as follows:

Step 1. Construct an FE model of the intact structure.

Step 2. Measure the lowest repeated natural frequency (ω_l^*) and its corresponding mode shape (φ_l^*) of the damaged structure.

Step 3. Normalise the obtained mode shape vectors of the analytical and damaged structure using (11).

Step 4. Determine healthy and damaged elements based on the R_l^* vector in (12).

Step 5. Create a new search space by removing healthy elements from all the elements.

Step 6. Use the lowest repeated closely-spaced modes (φ_l^*) of the healthy and damaged structures to construct the objective function (RMCE) of (27).

Step 7. Detect the damage severity of all identified damage elements from Step (4) in the optimisation problem of (27) using the PSO algorithm.

4. Numerical examples

Two numerical examples are considered to be solved to asses the capability of the proposed method which are: a 52-element spatial truss structure [53], and a 120-element spatial truss [54] structure. Note that the both examples of this paper are regarded as representatives of large-scale spatial structures for which the closely-spaced eigenvalues issue is investigated. The numerical examples are studied using different levels of the SNR. To this end, the applied structural mode shapes were contaminated by different noise percentage as discussed in Section 3.2.2. Reiterated, the probable damaged elements were identified from the list of all elements using the lowest repeated natural frequency (ω_l^*) and its corresponding mode shape (φ_l^*) from (12). Then, the PSO algorithm was employed to solve the second phase of the proposed method (damage quantification) through minimising the proposed optimisation problem (RMCE) of (27) for damage quantification. The specified parameters of the PSO algorithm to be used in this study are tabulated in Table 1.

Note that the damage was introduced to the elemental stiffness and mass matrices one at a time as degradation factors. As such, the stiffness and mass matrices were not affected by damage at the same time. The damage scenarios vary in terms of the location, severity and the type of fault in the defective elements. Moreover, two different states of the structure were considered for damage detection as follows:

1. without considering any mass retrofitted to the system.
2. considering some masses retrofitted to the system.

Note that the latter was introduced to the system in order to investigate the effect of the perturbation of the mass distribution to the enhancement of the closely-spaced eigenvalues problem which can further make the process of damage detection even more challenging. Usually, care must be taken when retrofitting a structure with structural components, components that affect overall stiffness of the structure. The retrofitted elements are thus often non-structural such as partition walls, windows, doors, etc. However, the aim of retrofitting the structures under study with masses was to show that even adding non-structural components can be problematic, when it comes to damage detection of the structures susceptible to closely-spaced eigenvalues phenomenon when retrofitted with extra masses. Therefore, there are totally four different cases to be considered for damage detection as follows:

Case 1: stiffness degradation without retrofitted masses to the structure.

Case 2: stiffness degradation with retrofitted masses to the structure.

Case 3: mass degradation without retrofitted masses to the structure.

Case 4: mass degradation with retrofitted masses to the structure.

4.1. The 52-member spatial truss

As the first example, the damage detection problem of 52-member spatial truss structure of Fig. 3 is considered to be solved via the proposed method in this section. The specifications of the truss model follows:

- 52 bar elements, 21 nodes, the total of 63 DoFs with 39 active DOFs remained after imposing the boundary conditions at the supports.

Table 1: The parameters of the PSO Algorithm.

Parameter	PSO
The number of particles	100
The maximum number of iterations	100
Cognitive parameter	2.1
Social parameter	1.9
Minimum of inertia weight	0.2
Minimum of inertia weight	0.9

Table 2: Damage scenarios of 52-member spatial truss

Case 1 (Stiffness Reduction)		Case 2 (Stiffness Reduction)		Case 3 (Stiffness Reduction)		Case 4 (Mass Reduction)	
Element No.	Ratio	Element No.	Ratio	Element No.	Ratio	Element No.	Ratio
2	0.15	10	0.10	14	0.20	6	0.35
19	0.20	26	0.25	19	0.10	16	0.20
23	0.30	38	0.30	22	0.30	27	0.25
45	0.20	40	0.30	40	0.25	33	0.20
		50	0.20	41	0.25	42	0.15
				52	0.20	48	0.35

- the cross section area of 0.01 m^2 identical for all elements.
- the modulus of elasticity and density of the material of respectively 2×10^{11} $\frac{\mathrm{N}}{\mathrm{m}^2}$ and 7420 $\frac{\mathrm{kg}}{\mathrm{m}^3}$.

Reiterated, damage was introduced to the elemental stiffness and mass matrices of the retrofitted and unretrofitted structures, with masses, one at a time as degradation factors (see Table 2). As such, damage scenarios of 1-3 present the stiffness reduction of the corresponding elements, whereas, the 4^{th} damage scenario corresponds to the mass reduction of the corresponding elements. In order to investigate whether or not the proposed method is sensitive to the number of defective elements, various number of defective elements was considered in different damage scenarios. Moreover, two states of the structure were considered, i.e. (1) without considering any mass perturbation, and (2) with retrofitting 50 kg lumped masses to all the unsupported node numbers of 1-13. We will further show, regarding the example of this section, that the problem of the repeated closely-spaced eigenvalues occurs when the mass distribution of the system is perturbed. Therefore, the proposed objective function (RMCE) of (27) is only applicable to this case in here.

Table 3 shows the 10 lowest natural frequencies of the structure obtained for all the damage scenarios. It is obvious from Table 3, as expected, that reducing the stiffness and mass matrices results in decreasing and increasing the natural frequencies in all the studied models, respectively.

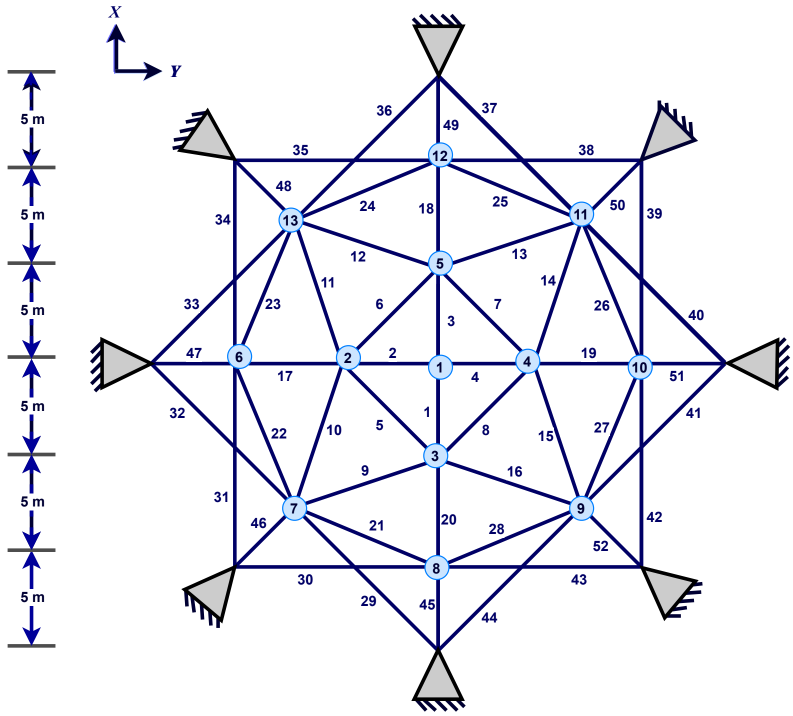

(a) Plan view

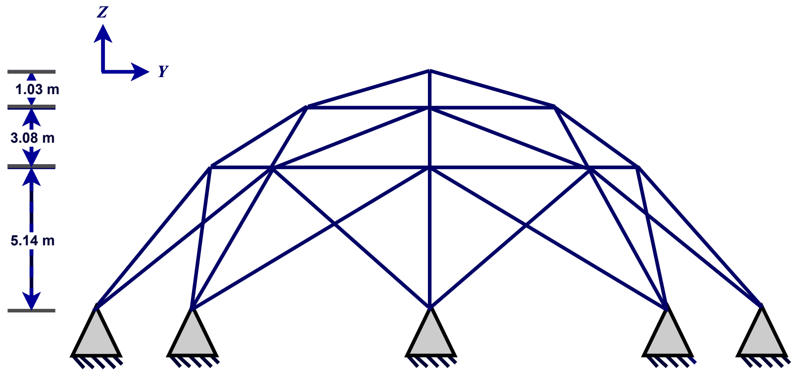

(b) Side view

Figure 3: The 52-member spatial truss.

Table 3: First ten natural frequencies of 52-member spatial truss retrofitted with lumped masses.

Case No.	Mode No.									
	1	2	3	4	5	6	7	8	9	10
Intact	24.6683	24.6683	34.0341	34.9976	44.7624	46.4770	52.6028	54.7488	59.4676	72.1273
Case 1	24.4775	24.4775	33.3019	34.5039	44.3597	45.8409	52.4222	54.6542	59.1073	70.2876
Case 2	24.2914	24.2914	33.7176	34.9227	44.6733	45.8333	52.4819	54.0809	59.1082	68.5942
Case 3	24.4610	24.4610	33.7914	34.5412	44.5786	45.4573	51.9588	54.4568	59.0549	70.5950
Case 4	24.9647	24.9647	34.4828	35.4404	44.9765	46.9672	52.9072	55.1141	59.9826	72.6288

Table 4: The $\mathrm{FDI}_{i,j}$ values for the first ten modes of the 52-member spatial truss retrofitted with lumped masses.

Mode No.	$\mathrm{FDI}_{i,j}$ (%)	Modal disparity	Identical
[1, 2]	5.65e-05	Very close	Yes
[2, 3]	31.91	Well-separated	No
[3, 4]	2.79	Close	No
[4, 5]	24.49	Well-separated	No
[5, 6]	3.76	Close	No
[6, 7]	12.37	Well-separated	No
[7, 8]	4.00	Close	No
[8, 9]	8.26	Separated	No
[9, 10]	19.24	Well-separated	No
[10, 11]	8.45	Separated	No

The studied 52-member spatial truss does not present the problem of closely-spaced eigenvalues without retrofitting any mass to it as depicted in Fig. 4a. However, the problem of closely-spaced eigenvalues occurs in several modes such as those circled regarding the five lowest natural frequencies of the structure (Fig. 4b). In some areas, even a cluster of closely-spaced resonances can be noted. This is more evident from Table 4 where the $\mathrm{FDI}_{i,j}$ values for ten lowest modes of the perturbed 52-bar spatial truss is presented. It can be also noted that the repetition of the modes happens regarding the first and second modes. Therefore, the first mode was used for damage detection in here.

4.1.1. Damaged localisation

As mentioned earlier, the first stage of the proposed damage detection method is dedicated to damage localisation. To this end, the modal residual vector explained in Section 3.1 was used. The 52-member spatial truss model considered here has 63 DOFs containing three translational DoFs at each node where only 39 DOFs are active. The noisy first mode data were only used for damage localisation in 3.1. Figs. 5 display the results of the obtained MRVBI at all active DOFs regarding the studied model with different

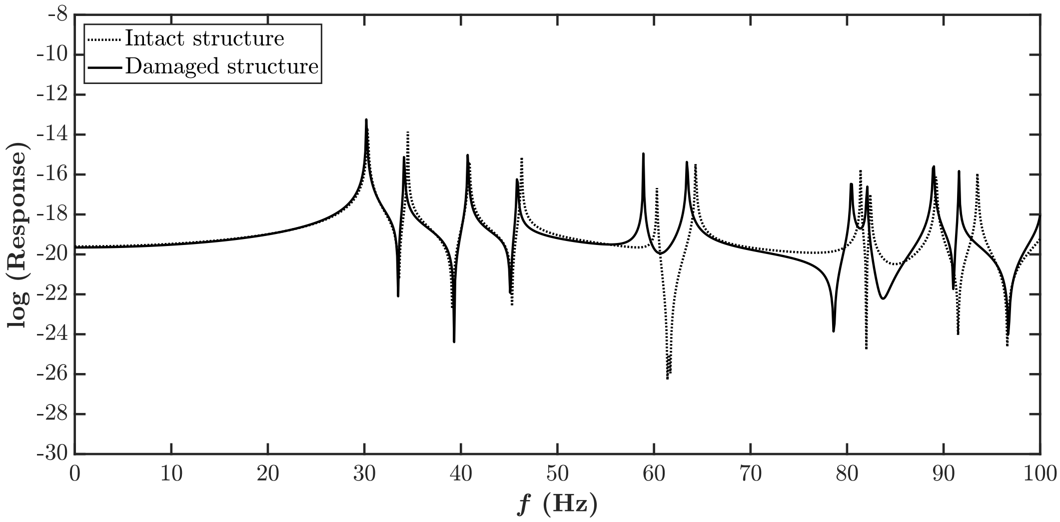

(a) Unperturbed

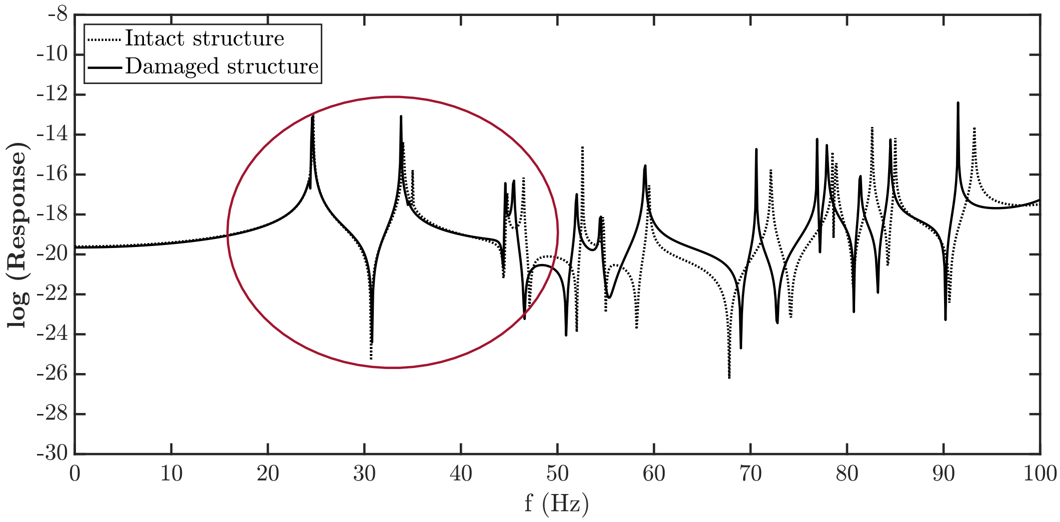

(b) Perturbed

Figure 4: The closely-spaced eigenvalues depicted in intact and damaged 52-member spatial truss for two cases of (a) unperturbed and (b) perturbed structure when the structure is excited at DoF 23 and the response is measured at DoF 30. Note that in case (a) the closely-spaced eigenvalues problem does not happen.

https://doi.org/10.1016/j.measurement.2021.110644

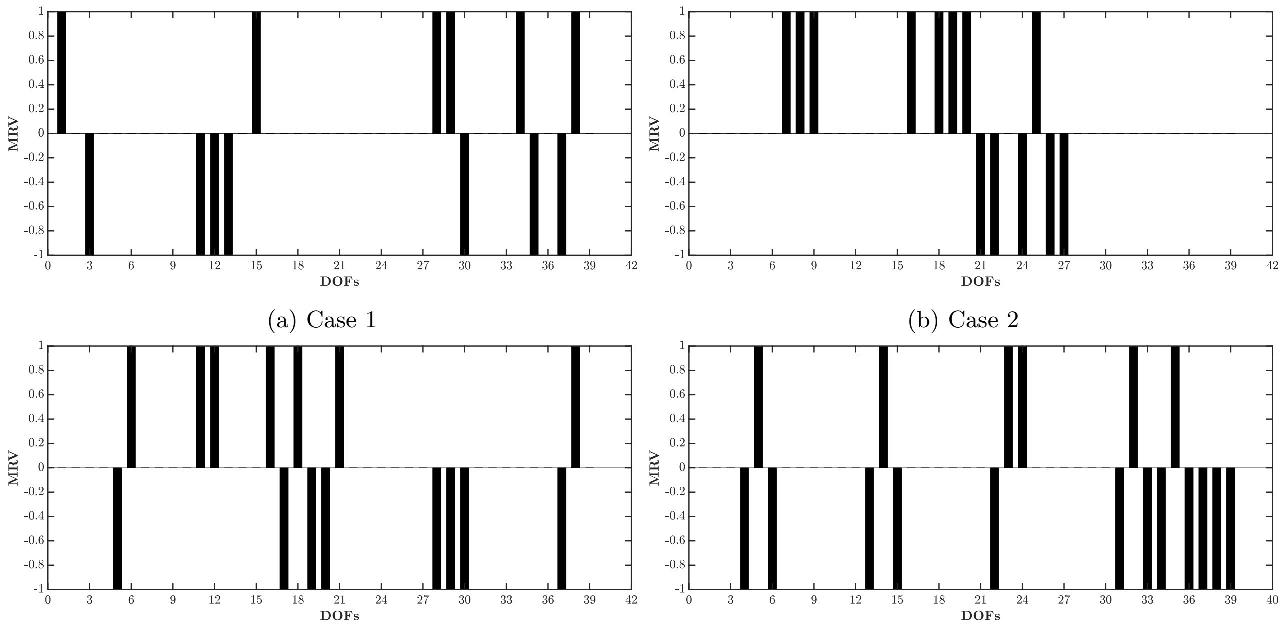

(a) Case 1 (b) Case 2

(c) Case 3 (d) Case 4

Figure 5: The MRVBI values for all DOFs corresponding to the nodes of 52-member spatial truss considering damage scenarios 1-4, using noisy data (SNR=16.48%). The values greater and less than zero were rounded respectively to 1 and -1 for better visualisation

.

damage cases 1-4 (Table 2), noisy measurements (15% noise, i.e. SNR=16.48), and mass perturbation (retrofitted with 50 kg lumped masses to all the active node numbers of 1-13). The DOFs corresponding to the non-zero values of MRVBI indicate the possible damaged elements. Table 5 shows the results of the damage localisation regarding each damage scenario. As can be seen from the table, all the defective elements were correctly identified.

4.1.2. Damage quantification

The identified defective elements from Section 4.1.1 were fed into the proposed optimisation problem of 27 to compute the severity of damage.

Figs. 6 show the obtained fitness results of solving the optimisation problem of (27) regarding all the damage scenarios. Table 6 outlines the obtained damage severity of the defective elements. It can be seen from the table that the proposed optimisation problem can compute the severity of damage in identified defective elements fairly accurately, using noisy data from the first mode only at the presence of the closely-spaced eigenvalues.

Finally, the accuracy indicators of all the damage scenarios were computed and presented in Table 7 (considering SNR=16.48%, SNR=20%). As such, the zero value of both FAE and DME demonstrates the precision of the damage localisation regarding the first stage of the proposed method. Regarding the second stage, RE and MSE values were obtained close to zero to further confirm the validity of the computed damage severity in defective elements.

https://doi.org/10.1016/j.measurement.2021.110644

Table 5: DOFs with non-zero values of MRVBI the corresponding damaged element of 52-member spatial truss considering damage scenarios 1-4 using noisy data (SNR=16.48%)

DoFs	Nodes	Elements
Scenario 1		
(1,2,3), (13,14,15)	1,5	2
(10,11,12), (28,29,30)	4,10	19
(28,29,30)	10,19	23
(34,35,36), (37,38,39)	12,13	45
Scenario 2		
(7,8,9), (19,20,21)	3,7	10
(25,26,27)	9,18	26
(16,17,18)	6,15	38
(19,20,21)	7,14	40
(7,8,9),(22,23,24)	3,8	50
Scenario 3		
(16,17,18), (37,38,39)	6,13	14
(10,11,12), (28,29,30)	4,10	19
(28,29,30)	10,17	22
(19,20,21)	7,14	40
(16,17,18)	6,14	41
(4,5,6),(16,17,18)	2,6	52
Scenario 4		
(4,5,6), (13,14,15)	2,5	6
(13,14,15), (31,32,33)	5,11	16
(22,23,24)	8,17	27
(37,38,39)	13,20	33
(31,32,33),(34,35,36)	11,12	42
(37,38,39)	13,21	48

4.2. The 120-member spatial truss

A 120-bar spatial truss of Figs. 7 is considered as the second example. The specification of the spatial truss studied in this section are listed as follows:

- A total of 49 joints and 147 DoFs, 111 of which remain active after imposing the boundary conditions.
- All members have equal cross section area of 0.01 m^2.
- The modulus of elasticity and the density of mass of 2×10^{11} $\frac{\mathrm{N}}{\mathrm{m}^2}$ and 7780 $\frac{\mathrm{kg}}{\mathrm{m}^3}$, respectively.

Table 6: Computed damage severity of the defective elements of 52-member spatial truss retrofitted with lumped masses (damage scenarios 1-4 using noisy data).

Case No.	Element No.	Actual damage	Predicted damage with different situation	
			$SNR = 20\%$	$SNR = 16.48\%$
1	2	0.15	0.1506	0.1589
	19	0.20	0.2008	0.2109
	23	0.30	0.3006	0.3123
	45	0.20	0.1991	0.1877
2	10	0.10	0.1008	0.1123
	26	0.25	0.2498	0.2403
	38	0.30	0.2998	0.3102
	40	0.30	0.3000	0.3097
	50	0.20	0.1988	0.2103
3	14	0.20	0.1989	0.2105
	19	0.10	0.1009	0.1108
	22	0.30	0.2989	0.3079
	40	0.25	0.2491	0.2478
	41	0.25	0.2507	0.2567
	52	0.20	0.1988	0.2043
4	6	0.35	0.3507	0.3472
	16	0.20	0.1987	0.2162
	27	0.25	0.2503	0.2388
	33	0.20	0.1985	0.2136
	42	0.15	0.1511	0.1391
	48	0.15	0.1485	0.1400

Table 7: Summary of the values of the error indices regarding the application of proposed method to 52-member spatial truss retrofitted with lumped masses (damage scenarios 1-4 using noisy data).

Case	$SNR = 20\%$				$SNR = 16.48\%$			
No.	DME	FAE	MSE	RE	DME	FAE	MSE	RE
1	Zero	Zero	0.0007	-0.1513	Zero	Zero	0.0111	-0.1733
2	Zero	Zero	0.0005	0.1507	Zero	Zero	0.0104	0.1215
3	Zero	Zero	0.0009	0.3021	Zero	Zero	0.0071	0.2708
4	Zero	Zero	0.0011	0.3017	Zero	Zero	0.0108	0.3039

https://doi.org/10.1016/j.measurement.2021.110644

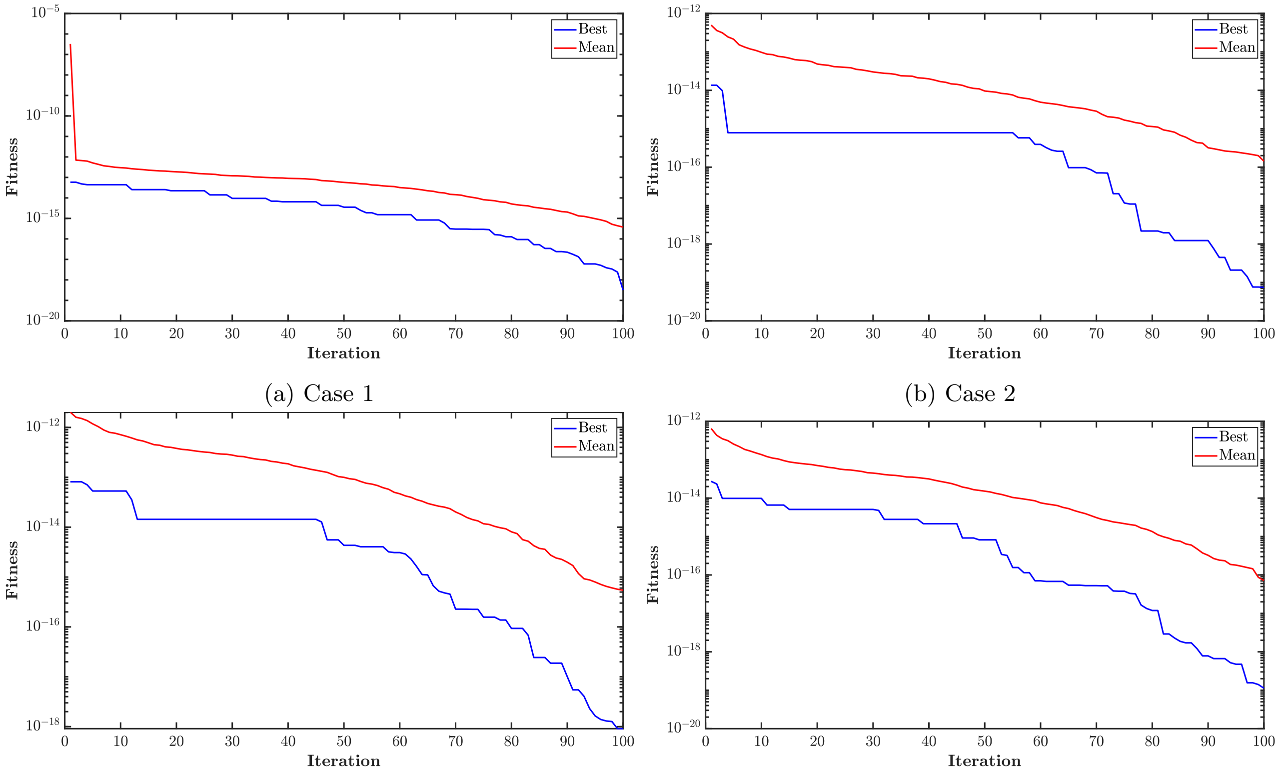

(a) Case 1 (b) Case 2

(c) Case 3 (d) Case 4

Figure 6: The variation of the objective function(RMCE) with the number of iterations of 52-member spatial truss considering damage scenarios 1-4 using noisy data (SNR=16.48%).

Likewise to the previous section, the sensitivity of the proposed method to the mass perturbation is investigated in here as well. To this end, concentrated masses were attached to all the unsupported nodes. As such, 100 kg lumped mass was attached to the node numbers 1-13 and 150 kg lumped mass was attached to the node numbers 14-37. Table 8 outlines the six damage scenarios with different damage severity regarding the loss of the stiffness (1-4) and the loss of the mass (5-6). The first 10 natural frequencies of the structure, regarding all the damage scenarios, were calculated and presented in Table 9. As expected, the natural frequencies decrease by stiffness reduction in scenarios 1-4 and increase with mass reduction in scenarios 5 and 6.

Unlike the previous example, the 120-member spatial truss presented in this section suffers from the closely-spaced eigenvalues problem even without having retrofitted with any lumped mass. Fig. 8 shows that there are quite a number of resonances that are closely-spaced for both cases of the structure without retrofitted masses (Figure 8a) and with retrofitted masses (Figure 8b). Table 10 presents the FDI measure calculated for some pair of modes within the ten first modes. It can be noted from Table 10 that in both cases the second mode is identified as the lowest repeated mode and therefore, is used for damage detection here.

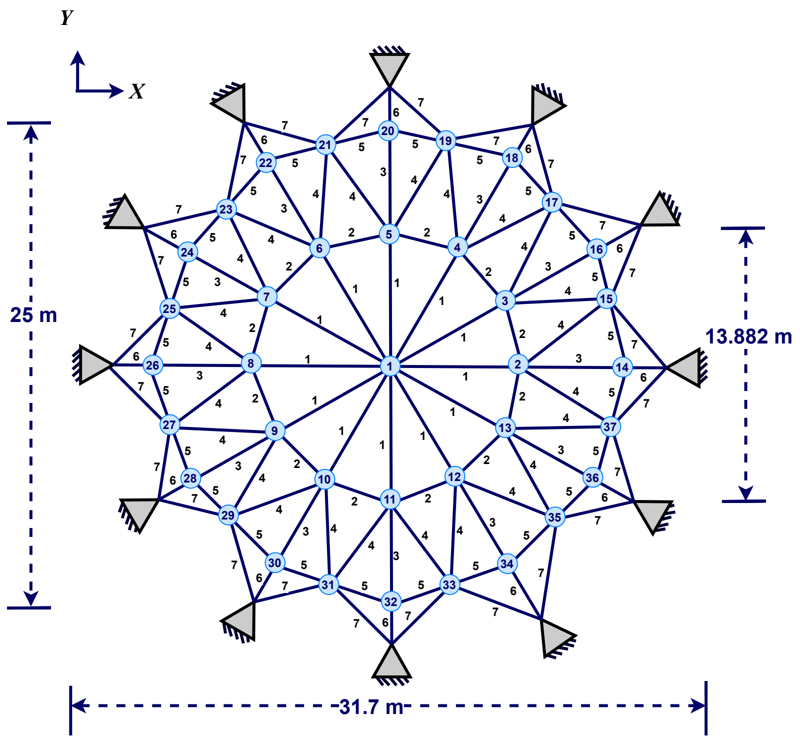

(a) Plan view

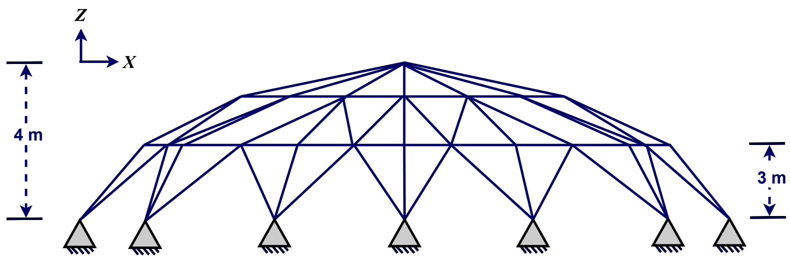

(b) Side view

Figure 7: The 120-member spatial truss [55]

.

Table 8: Damage scenarios of The 120-member spatial truss.(SR=Stiffness Reduction,MR=Mass Reduction)

Case 1 (SR)		Case 2 (SR)		Case 3 (SR)		Case 4 (SR)		Case 5 (MR)		Case 6 (MR)	
Element	Ratio	Element	Ratio	Element	Ratio	Element	Ratio	Element	Ratio	Element	Ratio
1	0.15	9	0.10	21	0.20	42	0.35	5	0.10	10	0.15
10	0.20	19	0.25	31	0.10	54	0.20	12	0.35	23	0.15
28	0.30	35	0.30	54	0.30	69	0.25	29	0.15	31	0.25
70	0.20	89	0.30	62	0.25	76	0.20	38	0.30	91	0.10
		91	0.20	101	0.25	81	0.15	102	0.25	99	0.30
				117	0.20	100	0.35	110	0.15	102	0.25

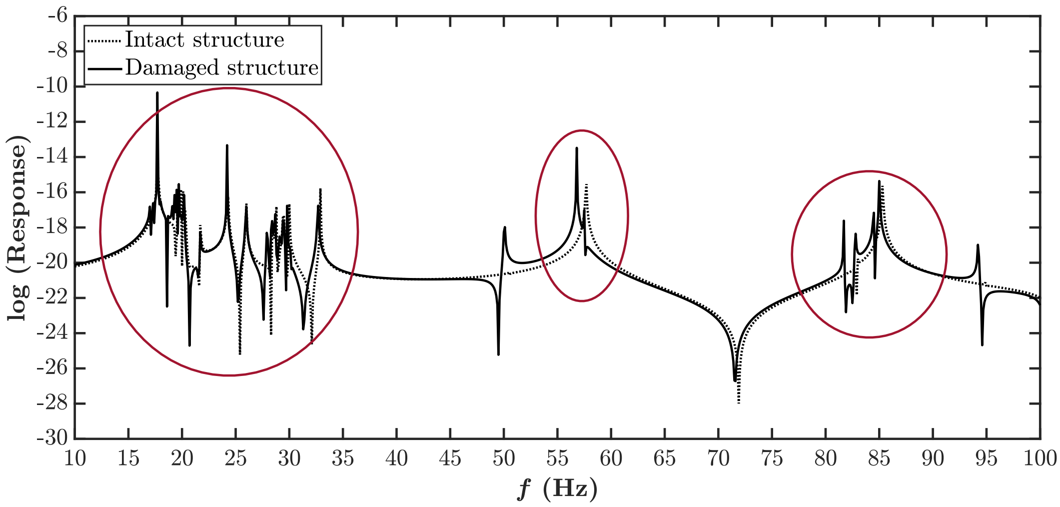

(a) Unperturbed

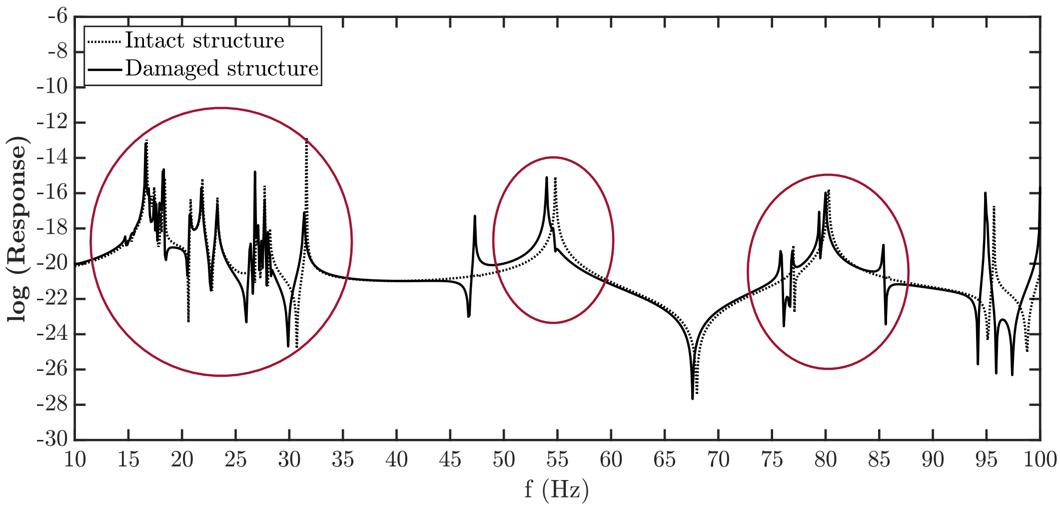

(b) Perturbed

Figure 8: The closely-spaced eigenvalues depicted in intact and damaged 120-member spatial truss for two cases of (a) unretrofitted, and (b) retrofitted structure when the structure is excited at DoF 21 and the response is measured at DoF 37.

Table 9: First ten natural frequencies of 120-member spatial truss retrofitted with lumped masses.

Lumped Masses		Mode No.									
		1	2	3	4	5	6	7	8	9	10
Intact	*Perturbed*	15.5514	15.6381	15.6381	15.9075	15.9775	16.1771	16.3913	16.5976	16.5977	17.4030
	Unperturbed	17.6177	17.7030	17.7030	17.7277	17.7277	17.9804	18.0623	18.7446	18.7446	19.3336
Case 1	*Perturbed*	15.1888	15.5777	15.5774	15.8485	15.9299	16.1631	16.3649	16.4747	16.5930	17.1928
	Unperturbed	17.1809	17.6379	17.6376	17.6993	17.7252	17.9205	18.0065	18.6028	18.7335	19.1615
Case 2	*Perturbed*	14.9531	15.4896	15.6313	15.7955	15.8768	16.1435	16.1435	16.4317	16.5254	16.9285
	Unperturbed	16.9068	17.4001	17.4007	17.6725	17.7094	17.9007	17.9889	18.5237	18.5959	18.7806
Case 3	*Perturbed*	15.4152	15.5213	15.5211	15.8138	15.8823	15.9415	16.2694	16.4684	16.5417	17.1315
	Unperturbed	17.3799	17.4825	17.4817	17.6161	17.6854	17.8927	17.9861	18.5839	18.6369	18.9735
Case 4	*Perturbed*	15.0559	15.3968	15.3967	15.7924	15.8255	15.9999	16.3287	16.4457	16.4696	17.1294
	Unperturbed	17.0196	17.5997	17.5997	17.6651	17.7059	17.8997	17.9381	18.5532	18.6062	19.0788
Case 5	*Perturbed*	15.5521	15.6389	15.6390	15.9086	15.9784	16.2671	16.4987	16.5989	16.5989	17.4378
	Unperturbed	17.6186	17.7063	17.7064	17.8354	17.8538	17.9832	18.0668	18.7499	18.7503	19.3826
Case 6	*Perturbed*	15.5811	15.6613	15.6618	15.9908	16.0244	16.2266	16.4748	16.5996	16.7241	17.4463
	Unperturbed	17.6526	17.7708	17.7701	17.7977	17.8387	18.0887	18.1577	18.7513	18.9145	19.4044

Table 10: The $\mathrm{FDI}_{i,j}$ values for the first ten modes of the 120-member spatial truss retrofitted with lumped masses (MD=Modal Disparity).

Mode No.	Closely spaced modes with different condition					
	Unperturbed			Perturbed		
	$\mathrm{FDI}_{i,j}$ (%)	MD	Identical	$\mathrm{FDI}_{i,j}$ (%)	MD	Identical
[1, 2]	0.5600	Very close	No	0.4830	Very close	No
[2, 3]	1.95e-06	Very close	Yes	1.16e-12	Very close	Yes
[3, 4]	1.7080	Close	No	0.1394	Very close	No
[4, 5]	0.4391	Very close	No	2.10e-14	Very close	Yes
[5, 6]	1.2415	Close	No	1.4154	Close	No
[6, 7]	1.3154	Close	No	0.4545	Very close	No
[7, 8]	1.2507	Close	No	3.7075	Close	No
[8, 9]	5.85e-06	Very close	Yes	1.78e-12	Very close	Yes
[9, 10]	4.7370	Close	No	3.0936	Close	No
[10, 11]	0.2926	Very close	No	0.5874	Very close	No

4.2.1. Damage localisation

The 120-member spatial truss model considered here has 147 translational DOFs, 111 DoFs of which are free when the boundary conditions are imposed. In the first step, MRVBI was used to locate the defective elements using noisy measurements from the second mode of the structure in (12). This was mainly due to the fact that the small value of the FDI (nearly close to zero), obtained for the second and third modes, suggests that these modes can be considered identical. Figs. 9 show the results of the obtained damage indicators at all DOFs for all the damage scenarios, i.e. 1-6. Note that adding the lumped masses in this case does not change the results of the damage localisation. The DOFs corresponding to the non-zero MRVBI indicate the possible damaged elements. Here, an element was considered defective, when the value of MRVBI corresponding to at least two DOFs of each of its nodes was obtained nonzero. Table 11 shows the damage sites in each damage scenario based upon the corresponding non-zero DOFs of the obtained MRVBI. Again, as can be seen from the table, all the damaged elements are identified correctly.

Table 11 shows the outcome of the damage localisation process. The results demonstrate that the applied method is robust to the application of noisy measurements from the second mode (the lowest repeated mode).

4.2.2. Damage quantification

The identified defective elements were used in the proposed optimisation problem of (27) to work out the damage severity of the defective elements. Figs. 10 show the convergence results of the optimisation problem regarding all the six damage scenarios when noisy data from the second mode (the lowest repeated mode) were used. Note that in order to avoid duplication, the results for the model retrofitted with masses are presented here only, though the results were literally the same for the case without any masses retrofitted to the structure. Table 12 presents the computed damage severity of the defective elements. It can be noted from the results that the proposed method is quite successful in damage quantification as well.

Table 13 lists the obtained accuracy measures of all the damage scenarios where the zero values of both FAE and DME demonstrate the perfect performance of the damage localisation. Also, having the value of RE and MSE obtained close to zero confirms that the proposed method is perfectly capable of damage quantification, using noisy measurements of the second mode only.

5. Comparison with other modal residual vector-based method

The accuracy of the proposed method was compared against two other well-known methods, namely TEDI [47] and FBDPI [48]. To this end, damage scenarios of 3 and 4 were only considered as examples of

Table 11: DOFs with non-zero values of MRVBI the cor-responding dam-aged element of 120-member spatial truss considering damage scenarios 1-6 using noisy data (SNR=16.48%).

DOFs	Nodes	Elements
Scenario 1		
(1,2,3), (4,5,6)	1,2	1
(1,2,3), (31,32,33)	1,11	10
(19,20,21), (70,71,72)	7,24	28
(67,68,69), (70,71,72)	23,24	70
Scenario 2		
(1,2,3), (28,29,30)	1,10	9
(10,11,12), (52,53,54)	4,18	19
(25,26,27), (85,86,87)	9,29	35
(49,50,51)	17,39	89
(52,53,54)	18,40	91
Scenario 3		
(13,14,15), (55,56,57)	5,19	21
(22,23,24), (76,77,78)	8,26	31
(19,20,21), (22,23,24)	7,8	54
(43,44,45), (46,47,48)	15,16	62
(73,74,75)	25,43	101
(103,104,105)	35,49	117
Scenario 4		
(34,35,36), (97,98,99)	12,33	42
(19,20,21), (22,23,24)	7,8	54
(64,65,66), (67,68,69)	22,23	69
(85,86,87), (88,89,90)	29,30	76
(100,101,102),(103,104,105)	34,35	81
(70,71,72)	24,43	100
Scenario 5		
(1,2,3), (16,17,18)	1,6	5
(1,2,3), (37,38,39)	1,13	12
(19,20,21), (73,74,75)	7,25	29
(28,29,30), (91,92,93)	10,31	38
(73,74,75)	25,44	102
(91,92,93)	31,46	110
Scenario 6		
(1,2,3), (31,32,33)	1,11	10
(13,14,15), (61,62,63)	5,21	23
(22,23,24), (76,77,78)	8,26	31
(52,53,54)	18,40	91
(67,68,69)	23,43	99
(73,74,75)	25,44	102

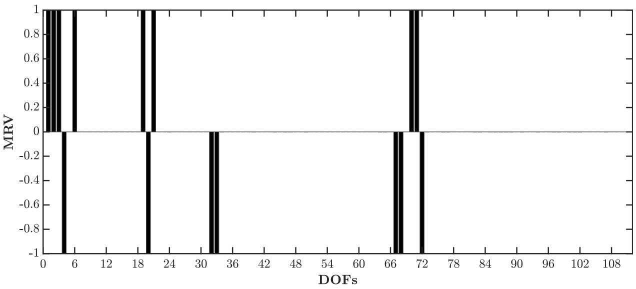

(a) Case 1

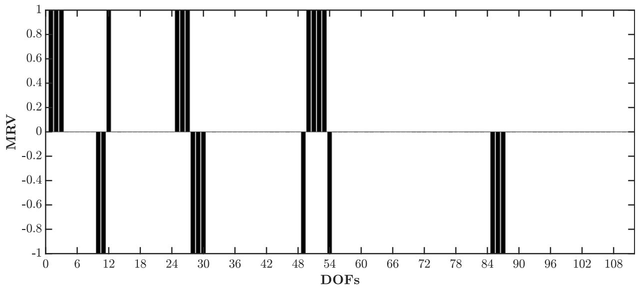

(b) Case 2

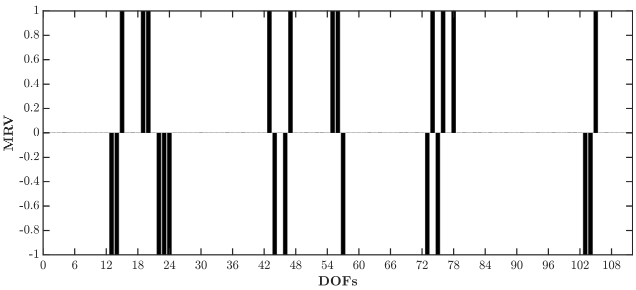

(c) Case 3

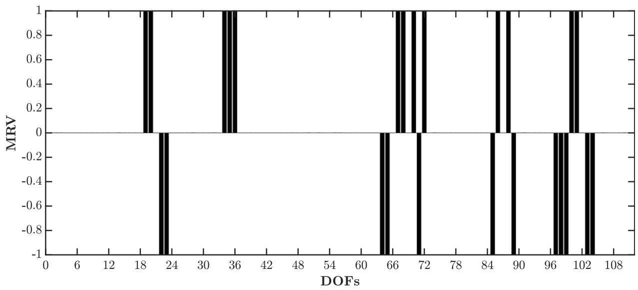

(d) Case 4

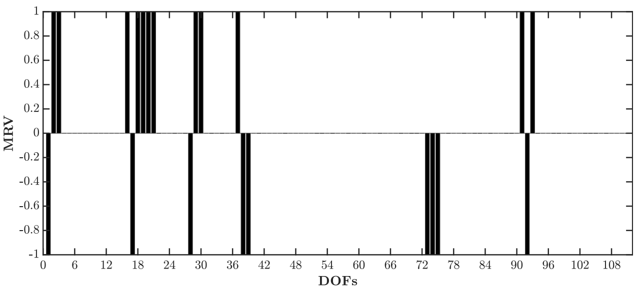

(e) Case 5

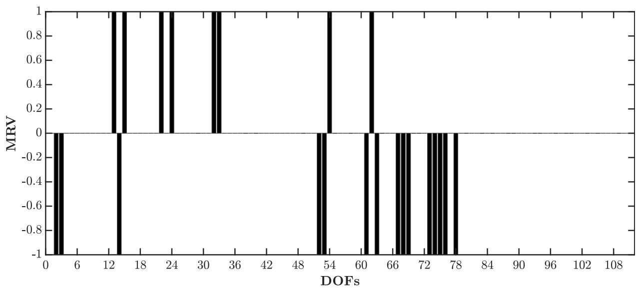

(f) Case 6

Figure 9: The MRVBI values for all DOFs corresponding to the nodes of 120-member spatial truss considering damage scenarios 1-6 using noisy data (SNR=16.48%). The values greater and less than zero were rounded respectively to 1 and -1 for better visualisation

.

Table 12: Damage severity of the defective elements of 120-member spatial truss considering damage scenarios 1-6 using noisy data (P=Perturbated , Unp=Unperturbated)

Case	Element	Actual	Predicted damage with different situation			
			U$np(SNR=20\%)$	U$np(SNR=16.48\%)$	P$(SNR=20\%)$	P$(SNR=16.48\%)$
1	1	0.15	0.1501	0.1503	0.1453	0.1423
	10	0.20	0.2002	0.1993	0.1963	0.1910
	28	0.30	0.3000	0.3003	0.3088	0.3099
	70	0.20	0.1998	0.1997	0.1938	0.1917
2	9	0.10	0.1000	0.1008	0.1086	0.1098
	19	0.25	0.2496	0.2508	0.2589	0.2600
	35	0.30	0.3007	0.2968	0.3087	0.3168
	89	0.30	0.3000	0.3006	0.3086	0.3108
	91	0.20	0.2003	0.1994	0.2096	0.1897
3	21	0.20	0.1997	0.2002	0.2108	0.2078
	31	0.10	0.1000	0.1008	0.1073	0.1089
	54	0.30	0.3000	0.2995	0.3089	0.2879
	62	0.25	0.2498	0.2492	0.2416	0.2403
	101	0.25	0.2500	0.2501	0.2568	0.2409
	117	0.20	0.2001	0.1994	0.1932	0.2101
4	42	0.35	0.3506	0.3494	0.3585	0.3410
	54	0.20	0.2002	0.1996	0.1897	0.2188
	69	0.25	0.2500	0.2506	0.2547	0.2436
	76	0.20	0.2000	0.1996	0.2046	0.1915
	81	0.15	0.1501	0.1504	0.1578	0.1592
	100	0.15	0.1500	0.1496	0.1536	0.1401
5	5	0.10	0.1001	0.1000	0.1047	0.1057
	12	0.35	0.3500	0.3503	0.3427	0.3407
	29	0.15	0.1500	0.1488	0.1475	0.1398
	38	0.30	0.2998	0.2996	0.2967	0.2962
	102	0.25	0.2500	0.2502	0.2565	0.2409
	110	0.15	0.1501	0.1496	0.1555	0.1430
6	10	0.15	0.1508	0.1507	0.1575	0.1538
	23	0.15	0.1498	0.1491	0.1484	0.1428
	31	0.25	0.2500	0.2499	0.2549	0.2399
	91	0.10	0.1000	0.1002	0.1088	0.1108
	99	0.30	0.3000	0.3002	0.3068	0.3092
	102	0.25	0.2500	0.2508	0.2446	0.2403

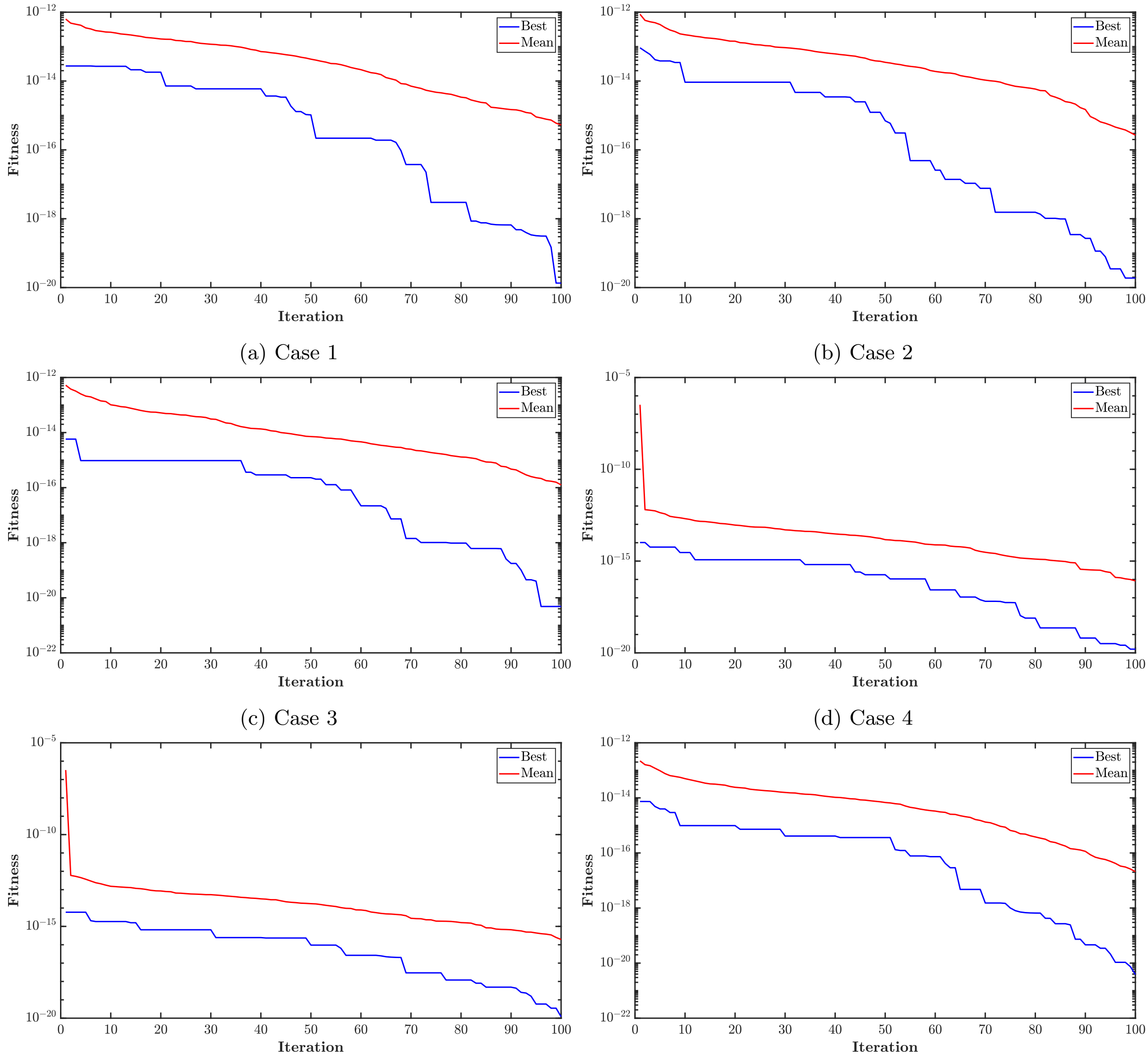

(a) Case 1

(b) Case 2

(c) Case 3

(d) Case 4

(e) Case 5

(f) Case 6

Figure 10: The variation of the objective function(RMCE) with the number of iterations of 120-member spatial truss considering damage scenarios 1-6 using noisy data (SNR=16.48%).

Table 13: Summary of the values of the error indices in the proposed approach of 120-member spatial truss considering damage scenarios 1-6 using noisy data .

Case	*Perturbed*				*Unperturbed*			
No.	DME	FAE	MSE	RE	DME	FAE	MSE	RE
SNR=20%								
1	Zero	Zero	0.0059	-0.1432	Zero	Zero	1.25e-04	-0.1501
2	Zero	Zero	0.0089	0.1114	Zero	Zero	2.80e-04	0.1495
3	Zero	Zero	0.0082	0.2857	Zero	Zero	1.00e-04	0.3003
4	Zero	Zero	0.0066	0.2855	Zero	Zero	1.50e-04	0.2993
5	Zero	Zero	0.0050	0.2972	Zero	Zero	6.67e-05	0.3000
6	Zero	Zero	0.0058	0.1825	Zero	Zero	1.67e-04	0.1995
SNR=16.48%								
1	Zero	Zero	0.0087	-0.1322	Zero	Zero	4.00e-04	-0.1495
2	Zero	Zero	0.0115	0.1177	Zero	Zero	0.0012	0.1514
3	Zero	Zero	0.0096	0.3032	Zero	Zero	5.00e-04	0.3006
4	Zero	Zero	0.0103	0.2968	Zero	Zero	4.67e-04	0.3006
5	Zero	Zero	0.0075	0.3259	Zero	Zero	4.17e-04	0.3012
6	Zero	Zero	0.0085	0.2027	Zero	Zero	4.84e-04	0.1992

damage as stiffness and mass degradation, respectively. The noisy data (SNR=16.48% and SNR=20%) of the first mode of the 52-member truss structure retrofitted with lumped masses and second mode of the 120-member truss structure retrofitted with and without lumped masses were used for damage detection using all the methods in this section. Table 14 and 15 compare the introduced error indices for the localisation and quantification results regarding all the methods. The large values of DME, FAE, MSE, and RE (Table 14 and 15) obtained from application of TEDI and FBDPI to both 52-member and 120-member spatial truss structures considering multiple damage cases (mass reduction and stiffness reduction) show the inaccuracy of the results of damage localisation and quantification using FBDPI and TEDI, demonstrating that these techniques do not work properly for the structures with closely-spaced eigenvalues. However, the low values of RE ,MSE ,DME and FAE (nearly zero) obtained for the results of the application of the proposed method to the aforementioned structures demonstrate the accuracy of the proposed method for damage detection in spatial truss structures with closely-spaced eigenvalues. Also, the proposed method is found to be less sensitive to the measurement noise compared with other methods demonstrating its applicability to real structures (Tables 7 and 13).

6. Conclusions

A two-stage damage detection method has been proposed for damage detection regarding structures with closely-spaced eigenvalues. The proposed method is based on the concept of residual force vector

Table 14: Comparison of the accuracy indicators for TEDI and FBDPI with proposed RMCE method of 52-member spatial truss considering damage scenarios 3, 4 (P=Perturbated).

Method	Scenario	Condition	DME	FAE	MSE	RE
(SNR=16.48%)						
FBDPI	3	P	0.22	0.27	0.52	-0.60
FBDPI	4	P	0.38	0.44	0.54	+0.72
TEDI	3	P	0.27	0.38	0.51	-0.56
TEDI	4	P	0.24	0.35	0.57	-0.65
RMCE	3	P	0	0	0.01	0.27
RMCE	4	P	0	0	0.01	0.30
(SNR=20%)						
FBDPI	3	P	0.16	0.15	0.49	-0.57
FBDPI	4	P	0.32	0.29	0.50	+0.70
TEDI	3	P	0.20	0.22	0.39	-0.59
TEDI	4	P	0.22	0.32	0.41	-0.63
RMCE	3	P	0	0	9.8e-04	0.30
RMCE	4	P	0	0	0.00	0.30

(the first phase) and optimisation of a newly constructed objective function (second phase). The probable defective elements were first identified in the first phase to reduce the dimensionality of the search space regarding the second phase. The second phase of the proposed method was based on the fact that a map can be established between the modes of the damaged and undamaged structures with closely-spaced eigenvalues. Two examples of 52-member and 120-member spatial trusses were solved in this paper to investigate the capability of the proposed two-stage damage detection method. Two types of damage scenarios were considered in general, i.e. mass degradation and stiffness degradation. It is known that structure retrofitted with nonstructural components throughout their service life resulting in more severe closely-spaced eigenvalues problem in their response. Therefore, two states of the structure were considered in this paper which are: (1) the unretrofitted structure and (2) the retrofitted structure with lumped masses. It was shown that the 52-member truss does not present the closely-spaced eigenvalues problem, however, when retrofitted with some lumped masses, the problem of the closely-spaced eigenvalues comes into existence. However, regarding the 120-member spatial truss structure, both retrofitted and unretrofitted structures suffer from the closely-spaced eigenvalues problem. Therefore, the proposed method is applicable to the retrofitted 52-member truss and retrofitted and unretrofitted 120-member truss structures. The information from the lowest repeated mode was shown to be enough for damage detection. We showed that the proposed method can be successfully used for damage detection in spatial truss structures when the closely-spaced eigenvalues problem occurs. The proposed method was also

Table 15: Comparison of the accuracy indicators for TEDI and FBDPI with the proposed RMCE method applied to the 120-member spatial truss retrofitted with lumped masses (damage scenarios 3 and 4, P=Perturbated , Unp=Unperturbated).

Method	Scenario	Condition	DME	FAE	MSE	RE
(SNR=16.48%)						
FBDPI	3	P	0.28	0.30	0.54	+0.62
FBDPI	3	Unp	0.30	0.22	0.40	+0.79
FBDPI	4	P	0.44	0.69	0.49	-0.61
FBDPI	4	Unp	0.49	0.51	0.46	-0.66
TEDI	3	P	0.39	0.49	0.62	-0.52
TEDI	3	Unp	0.34	0.22	0.41	+0.73
TEDI	4	P	0.39	0.51	0.50	-0.70
TEDI	4	Unp	0.17	0.45	0.47	-0.60
RMCE	3	P	0	0	0.01	0.30
RMCE	3	Unp	0	0	5.e-04	0.30
RMCE	4	P	0	0	0.01	0.30
RMCE	4	Unp	0	0	4.7e-04	0.30
(SNR=20%)						
FBDPI	3	P	0.18	0.14	0.32	+0.53
FBDPI	3	Unp	0.21	0.17	0.33	+0.61
FBDPI	4	P	0.41	0.57	0.43	-0.57
FBDPI	4	Unp	0.48	0.36	0.35	-0.60
TEDI	3	P	0.44	0.39	0.37	-0.50
TEDI	3	Unp	0.39	0.23	0.37	+0.68
TEDI	4	P	0.25	0.31	0.34	-0.54
TEDI	4	Unp	0.10	0.39	0.37	-0.59
RMCE	3	P	0	0	0.01	0.29
RMCE	3	Unp	0	0	1e-04	0.30
RMCE	4	P	0	0	0.01	0.29
RMCE	4	Unp	0	0	1.5e-04	0.30

compared with two other damage detection methods and its superiority in damage detection of structures with closely-spaced eigenvalues problem was demonstrated through evaluating the performance of the methods using some performance criteria.

The authors, however, are well aware of the limitation of the numerical studies and aim to validate their findings through conducting experimental studies in their future work.

References

[1] Liu, Y., Hong, X., Zhang, B.. A novel velocity anisotropy probability imaging method using ultrasonic guided waves for composite plates. Measurement 2020;166:108087. doi:10.1016/j.measurement.2020.108087.

[2] Mousavi, M., Taskhiri, M.S., Holloway, D., Olivier, J., Turner, P.. Feature extraction of wood-hole defects using empirical mode decomposition of ultrasonic signals. NDT & E International 2020;114:102282. doi:10.1016/j.ndteint.2020.102282.

[3] Zheng, G., Zhao, W., Tian, Y., Liu, C., Zheng, B.. Structural-damage localization using ultrasonic guided waves based on the lossless filtering method. Smart Materials and Structures 2020;29(7):075024. doi:10.1088/1361-665x/ab8b2f.

[4] Shi, L., Lu, Y., Guan, R.. Detection of crack development in steel fibre engineered cementitious composite using electrical resistivity tomography. Smart Materials and Structures 2019;28(12):125011. doi:10.1088/1361-665X/AB5047.

[5] Tian, Y., Shen, Y., Rao, D., Xu, W.. Metamaterial improved nonlinear ultrasonics for fatigue damage detection. Smart Materials and Structures 2019;28(7):075038. doi:10.1088/1361-665X/AB2566.

[6] Wang, B., Zhong, S., Lee, T.L., Fancey, K.S., Mi, J.. Non-destructive testing and evaluation of composite materials/structures: A state-of-the-art review. Advances in Mechanical Engineering 2020;12(4):1–28. doi:10.1177/1687814020913761.

[7] Downes, G.M., Lausberg, M., Potts, B., Pilbeam, D., Bird, M., Bradshaw, B.. Application of the iml resistograph to the infield assessment of basic density in plantation eucalypts. Australian Forestry 2018;81(3):177–185. doi:10.1080/00049158.2018.1500676.

[8] Mousavi, M., Gandomi, A.H.. An input-output damage detection method using static equivalent formulation of dynamic vibration. Archives of Civil and Mechanical Engineering 2018;18:508–514. doi:10.1016/j.acme.2017.01.007.

[9] Wang, X., Zhang, G., Wang, X., Ni, P.. Output-only structural parameter identification with evolutionary algorithms and correlation functions. Smart Materials and Structures 2020;29(3):035018. doi:10.1088/1361-665X/AB6CE9.

[10] Mousavi, M., Holloway, D., Olivier, J., Alavi, A.H., Gandomi, A.H.. A shannon entropy approach for structural damage identification based on self-powered sensor data. Engineering Structures 2019;200:109619. doi:10.1016/j.engstruct.2019.109619.

[11] Mousavi, M., Holloway, D., Olivier, J., Gandomi, A.H.. Beam damage detection using synchronisation of peaks in instantaneous frequency and amplitude of vibration data. Measurement 2021;168:108297.

[12] Mousavi, M., Gandomi, A.H.. A hybrid damage detection method using dynamic-reduction transformation matrix and modal force error. Engineering Structures 2016;111:425–434. doi:10.1016/j.engstruct.2015.12.033.

[13] Sharif-Khodaei, Z., Aliabadi, M.. Assessment of delay-and-sum algorithms for damage detection in aluminium and composite plates. Smart materials and structures 2014;23(7):075007. doi:10.1088/0964-1726/23/7/075007.

[14] Dahak, M., Touat, N., Kharoubi, M.. Damage detection in beam through change in measured frequency and undamaged curvature mode shape. Inverse Problems in Science and Engineering 2019;27(1):89–114. doi:10.1080/17415977.2018.1442834.

[15] Souza, M., Castello, D., Roitman, N., Ritto, T.. Impact of damping models in damage identification. Shock and Vibration 2019;2019. doi:10.1155/2019/4652328.

[16] Lestari, W., Qiao, P., Hanagud, S.. Curvature mode shape-based damage assessment of carbon/epoxy composite beams. Journal of intelligent material systems and structures 2007;18(3):189–208. doi:10.1177/1045389X06064355.

[17] Kumar, M., Shenoi, R., Cox, S.. Experimental validation of modal strain energies based damage identification method for a composite sandwich beam. Composites Science and Technology 2009;69(10):1635–1643. doi:10.1016/j.compscitech.2009.03.019.

[18] Yang, Q., Liu, J.. Damage identification by the eigenparameter decomposition of structural flexibility change. International Journal for Numerical Methods in Engineering 2009;78(4):444–459. doi:10.1002/nme.2494.

[19] Wu, D., Law, S.. Model error correction from truncated modal flexibility sensitivity and generic parameters: part i—simulation. Mechanical Systems and Signal Processing 2004;18(6):1381–1399. doi:10.1016/S0888-3270(03)00094-3.

[20] Pandey, A., Biswas, M.. Damage detection in structures using changes in flexibility. Journal of sound and vibration 1994;169(1):3–17. doi:10.1006/jsvi.1994.1002.

[21] Yang, Q.. A new damage identification method based on structural flexibility disassembly. Journal of Vibration and Control 2011;17(7):1000–1008. doi:10.1177/1077546309360052.

[22] Esfandiari, A., Nabiyan, M.S., Rofooei, F.R.. Structural damage detection using principal component analysis of frequency response function data. Structural Control and Health Monitoring 2020;27(7):e2550. doi:10.1002/stc.2550.

[23] Richiedei, D., Tamellin, I., Trevisani, A.. Simultaneous assignment of resonances and antiresonances in vibrating systems through inverse dynamic structural modification. Journal of Sound and Vibration 2020;485:115552. doi:10.1016/j.jsv.2020.115552.

[24] Faravelli, L., Casciati, S.. Structural damage detection and localization by response change diagnosis. Progress in Structural Engineering and Materials 2004;6(2):104–115. doi:10.1002/pse.171.

[25] Mohan, S., Maiti, D.K., Maity, D.. Structural damage assessment using frf employing particle swarm optimization. Applied Mathematics and Computation 2013;219(20):10387–10400. doi:10.1016/j.amc.2013.04.016.

[26] Porcu, M., Patteri, D., Melis, S., Aymerich, F.. Effectiveness of the frf curvature technique for structural health monitoring. Construction and Building Materials 2019;226:173–187. doi:10.1016/j.conbuildmat.2019.07.123.

[27] Shadan, F., Khoshnoudian, F., Esfandiari, A.. A frequency response-based structural damage identification using model updating method. Structural Control and Health Monitoring 2016;23(2):286–302. doi:10.1002/stc.1768.

[28] Niu, Z.. Frequency response-based structural damage detection using gibbs sampler. Journal of Sound and Vibration 2020;470:115160. doi:10.1016/j.jsv.2019.115160.

[29] Razavi, M., Hadidi, A.. Assessment of sensitivity-based fe model updating technique for damage detection in large space structures. Structural Monitoring and Maintenance 2020;7(3):261–281. doi:10.12989/smm.2020.7.3.261.

[30] KIM, H., BARTKOWICZ, T.. Damage detection and health monitoring of large space structures. In: 34th Structures, Structural Dynamics and Materials Conference. 1993, p. 1705. doi:10.2514/6.1993-1705.

[31] Mousavi, M., Holloway, D., Olivier, J., Gandomi, A.H.. A baseline-free damage detection method using vbi incomplete measurement data. Measurement 2021;174:108957. doi:10.1016/j.measurement.2020.108957.

[32] Kang, F., Li, J.j., Xu, Q.. Damage detection based on improved particle swarm optimization using vibration data. Applied Soft Computing 2012;12(8):2329–2335. doi:10.1016/j.asoc.2012.03.050.

[33] Khatir, S., Wahab, M.A.. A computational approach for crack identification in plate structures using xfem, xiga, pso and jaya algorithm. Theoretical and Applied Fracture Mechanics 2019;103:102240. doi:10.1016/j.tafmec.2019.102240.

[34] Jiang, Y., Wang, S., Li, Y.. Localizing and quantifying structural damage by means of a beetle swarm optimization algorithm. Advances in Structural Engineering 2021;24(2):370–384. doi:10.1177/1369433220956829.

[35] Wei, Z., Liu, J., Lu, Z.. Structural damage detection using improved particle swarm optimization. Inverse Problems in Science and Engineering 2018;26(6):792–810. doi:10.1080/17415977.2017.1347168.

[36] Dinh-Cong, D., Vo-Duy, T., Ho-Huu, V., Dang-Trung, H., Nguyen-Thoi, T.. An efficient multi-stage optimization approach for damage detection in plate structures. Advances in Engineering Software 2017;112:76–87. doi:10.1016/j.advengsoft.2017.06.015.

[37] Naderi, A., Sohrabi, M.R., Ghasemi, M.R., Dizangian, B.. A swift technique for damage detection of determinate truss structures. Engineering with Computers 2020;:1–9doi:10.1007/s00366-020-00940-0.

[38] Vo-Duy, T., Ho-Huu, V., Dang-Trung, H., Nguyen-Thoi, T.. A two-step approach for damage detection in laminated composite structures using modal strain energy method and an improved differential evolution algorithm. Composite Structures 2016;147:42–53. doi:10.1016/j.compstruct.2016.03.027.

[39] Xiang, J., Liang, M.. A two-step approach to multi-damage detection for plate structures. Engineering Fracture Mechanics 2012;91:73–86. doi:10.1016/j.engfracmech.2012.04.028.

[40] Bernal, D.. Closely spaced roots and defectiveness in second-order systems. Journal of engineering mechanics 2005;131(3):276–281. doi:10.1061/~ASCE!0733-9399~2005!131:3~276!

[41] Ghosh, D., Ghanem, R.. An invariant subspace-based approach to the random eigenvalue problem of systems with clustered spectrum. International journal for numerical methods in engineering 2012;91(4):378–396. doi:10.1002/nme.4276.

[42] Brincker, R., Lopez-Aenlle, M.. Mode shape sensitivity of two closely spaced eigenvalues. Journal of Sound and Vibration 2015;334:377–387. doi:10.1016/j.jsv.2014.08.015.

[43] Au, S.K., Brownjohn, J.M., Li, B., Raby, A.. Understanding and managing identification uncertainty of close modes in operational modal analysis. Mechanical Systems and Signal Processing 2021;147:107018. doi:10.1016/j.ymssp.2020.107018.

[44] Brincker, R., Skafte, A., López-Aenlle, M., Sestieri, A., D'Ambrogio, W., Canteli, A.. A local correspondence principle for mode shapes in structural dynamics. Mechanical Systems and Signal Processing 2014;45(1):91–104.

[45] Yang, Q., Liu, J.. Structural damage identification based on residual force vector. Journal of sound and vibration 2007;305(1-2):298–307. doi:10.1016/j.jsv.2007.03.033.

[46] Li, H., Lu, Z., Liu, J.. Structural damage identification based on residual force vector and response sensitivity analysis. Journal of Vibration and Control 2016;22(11):2759–2770. doi:10.1177/1077546314549822.

[47] Nobahari, M., Ghasemi, M., Shabakhty, N.. A fast and robust method for damage detection of truss structures. Applied Mathematical Modelling 2019;68:368–382. doi:10.1016/j.apm.2018.11.025.

[48] Seyedpoor, S., Montazer, M.. A damage identification method for truss structures using a flexibility-based damage probability index and differential evolution algorithm. Inverse Problems in Science and Engineering 2016;24(8):1303–1322. doi:10.1080/17415977.2015.1101761.

[49] Cancelli, A., Laflamme, S., Alipour, A., Sritharan, S., Ubertini, F.. Vibration-based damage localization and quantification in a pretensioned concrete girder using stochastic subspace identification and particle swarm model updating. Structural Health Monitoring 2020;19(2):587–605. doi:https://doi.org/10.1177/1475921718820015.

[50] He, W.Y., Ren, W.X., Zhu, S.. Damage detection of beam structures using quasi-static moving load induced displacement response. Engineering Structures 2017;145:70–82. doi:10.1016/j.engstruct.2017.05.009.

[51] The MathWorks, I.. Global Optimization Toolbox. Natick, Massachusetts, United State; 2020.

[52] Dos Santos, J.A., Soares, C.M., Soares, C.M., Maia, N.. Structural damage identification in laminated structures using frf data. Composite Structures 2005;67(2):239–249. doi:10.1016/j.compstruct.2004.09.011.

[53] Naseralavi, S., Salajegheh, E., Salajegheh, J., Fadaee, M.. Detection of damage in cyclic structures using an eigenpair sensitivity matrix. Computers & structures 2012;110:43–59. doi:10.1016/j.compstruc.2012.06.003.

[54] Soh, C.K., Yang, J.. Fuzzy controlled genetic algorithm search for shape optimization. Journal of computing in civil engineering 1996;10(2):143–150. doi:10.1061/(ASCE)0887-3801(1996)10:2(143).

[55] Hassani, S., Shadan, F.. Using incomplete frf measurements for damage detection of structures with closely-spaced eigenvalues. Measurement 2021;:110388doi:https://doi.org/10.1016/j.measurement.2021.110388.